Crustal modeling in the Naeen region

Z.S. Riazi Rad

Islamic Azad University, Chalus branch
zohrehriazi@srbiau.ac.ir

Abstract

This study, joint inversion method of body waves and receiver function, has been investigated. At first body waves recorded in broadband Naein station, have been analyzed with one station and two station methods. Therefore, travel time curves and body wave velocities of crust and upper mantel indicated. These method-calculated depths of Moho discontinue (40 km). The receiver function method has been divided upper, middle and lower crust. Upper, middle and lower crust thickness is 14 km, Vp=3.9-4.6 km/s, h=6 km, Vp=4.8-5.9 km/s and h=19km, Vp=3.7-4.6 km/s. depth of Moho discontinue with joint inversion calculated 38km. this method show two layers (upper and lower crust). Vp=6.2-6.7 km/s, Vs=3.6-3.7 km/s and h=12km in upper crust and Vp=6.7-8.01 km/s, Vs=3.7-4.6 km/s and h= 26km. The crustal velocity coincides with the region of high seismic activity, which indicates that the crustal anomaly is related to active tectonic processes.

Keywords*: Modeling, Crust, joint inversion, Central Iran*

Introduction

The problem of data-driven velocity model building for depth-imaging applications is approached from the point of view of simultaneous joint inversion of separate geophysical domains. For this purpose, a general formulation of the joint inversion problem is provided. The method is then applied to a real (long offsets) seismic dataset from Central Iran where seismic refraction travel-time residuals (first-break and Common Image Gather residuals) are jointly inverted with receiver function for improving velocity model building and the corresponding depth-domain seismic image.

Effective depth imaging through migration can be achieved only if a precise estimate of interval velocity in depth is available. The definition of a reliable velocity model for depth imaging is a difficult task especially when sharp lateral and vertical velocity variations are present. The problem becomes even more serious when the seismic refraction data are noisy giving little chance to extract useful velocity information from the data. Geologic models can provide a guide to the velocity model building and data integration with other geophysical methods can also be extremely important. Several different approaches to geophysical data integration were proposed in the past but in a very few cases the data integration problem has been handled in terms of simultaneous joint inversion of geophysical data. No applications to date, however, attempted the simultaneous joint inversion of non-seismic geophysical data and pre-stack seismic migration residuals for the improvement of seismic images in depth domain.

Formulation of the Joint Inverse Problem

The conversion of one elastic wave, either P or S, into another upon reflection or transmission at an interface is described by the *Zoeppritz equations.* These equations are algebraically quite complex and it is not practical to reproduce them here.

$$PN=\frac{1}{2}\left(1-4P^2\right)\frac{\Delta\rho}{\rho}+\frac{1}{2\cos^2 i}\frac{\Delta\alpha}{\alpha}$$

$$RF=-\frac{\alpha P}{2\cos j}\left(1-2\beta^2P^2+\frac{2\beta\cos i\cos j}{\alpha\beta}\right)\frac{\Delta\rho}{\rho}-\left(4\beta^2P^2-\frac{4\beta\cos i\cos j}{\alpha\beta}\right)\frac{\Delta\beta}{\beta}$$

Instead, we will present useful concepts and approximate forms. Since there are four possible incident waves, upcoming, downcoming P, S, and four possible scattered waves, upgoing, and downgoing P and S, sixteen scattering coefficients link them. The normal incidence P_N can be written in other suggestive ways. If we define the *impedance contrast* $\Delta I=I_2-I_1$, and the *average impedance* $I=(I_2+I_1)/2$, then $P_N=0.5\Delta I/I$. Going further, since P-wave impedance is the product of density, ρ, and P-wave velocity, α, it turns out that $P_N=.5(\Delta_\alpha/\alpha+\Delta_\rho/\rho)$. The ratios in the parenthesis are called the *P-wave velocity fluctuation,* $f_\alpha=\Delta\alpha/\alpha$, and the *density fluctuation*, $f_\rho=\Delta\rho/\rho$, so that $P_N=.5f_\alpha+.5f_\rho$. This suggests the very useful *Colombo approximation* that $P_N\approx C_\alpha f_\alpha+C_\rho f_\rho+C_\beta f_\beta$. Here f_β is the *S-wave velocity fluctuation* and the coefficients C_α, C_ρ, C_β depend upon the P-wave and S-wave incidence and refraction angles and the average αβρbut not upon ΔαΔβΔρ.

Comparing the normal incidence form of P_N to the Colombo approximation shows that, for an incidence angle of 0^0, $C_\alpha=C_\rho=.5$ and $C_\beta=0$. So at normal incidence, P_N carries information about f_α and f_ρ in equal amounts and nothing at all about f_β . This situation changes as we move to nonzero offset and C_α, C_ρ, C_β depart from their normal values of (.5,.5,0). If we let θdenote the average of the P-wave angles of incidence and transmission and φbe the average of the S-wave angles of reflection and transmission, then the variation of C_α, C_ρ, C_β with offset can be represented either as dependence on θor upon φsince these angles are related by Snell's law. In addition, C_ρ, C_β are not independent of one another in fact $C_\rho=.5+.5C_\beta$. Precisely how these coefficients vary depends upon the specific values of the elastic constants. These cases are idealized examples of the regional and reservoir behavior, at the stratigraphic level of the top of the channel, in the Blackfoot field. In both reservoir and regional settings, the fluctuations f_α ,f_ρ ,f_β have the same sign with αand ρ decreasing while βincreases. However, the magnitude of these changes is much great in the reservoir case.

Figure 1 shows the behavior of of C_α,C_ρ,C_β for both the reservoir and non-reservoir cases. Colombo also provides an approximate form for the refraction coefficient for a P-wave converting to and S-wave as $RF\approx d_\beta f_\beta+d_\rho f_\rho$. As before, the coefficients d_β, d_ρ depend upon either the P-wave angle θor the S-wave angle φand the average (background) elastic parameters. As with the P-wave case, the density and S-wave coefficients are not completely independent though the relation between them is more complicated: $d_\rho=-sin\ \theta/(2\cos\varphi)+.5d_\beta$. Figure 2 shows the behavior of d_β ,d_ρ versus P-wave incidence angle and, again, the curves change very little from the regional to the reservoir scenario.

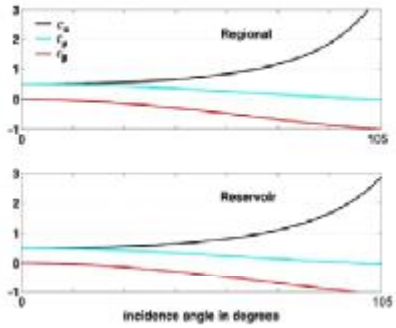

Figure 1. The coefficients C_α, C_ρ, C_β of the Colombo approximation $P_N \approx C_\alpha f_\alpha + C_\rho f_\rho + C_\beta f_\beta$ are shown as a function of the incidence angle.

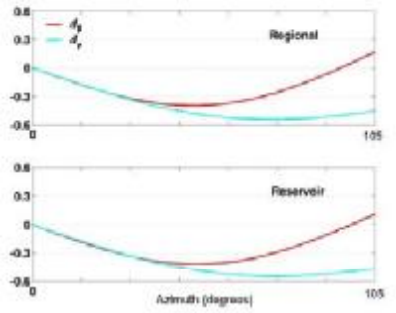

Figure 2. The coefficients d_β ,d_ρ of the Colombo approximation $RF \approx d_\beta f_\beta + d_\rho f_\rho$ are shown versus P-wave azimuth angle.

That is, f_α can be estimated, in principle, by an equation of the form

$$f_a = \sum_k a(\theta_k) PN + \sum_k b(\theta_k) RF$$

With similar equations, having different weighting functions, for f_β , f_ρ. In this equation, the sum is over all available offsets and the weights, $a(\theta_k)$, are known functions of the background velocity and the incidence angle for the k^{th} offset and $b(\theta_k)$ are the weights for the receiver function data. Similar equations, with different weights, will estimate f_β or f_ρ. The weights for the P_N refraction data $a(\theta_k)$ in these expressions are generally quite different from the analogous weights in the inversion using P_N data alone.

Seismic data were initially processed in time domain using well-established techniques such-as tomographic static calculation (i.e. tomostatics), multi-window deconvolution and state-of-the-art residual statics and denoising algorithms. The pre-processed data were then provided for the depth-imaging phase. Receiver function data were processed in a robust and fairly standard processing approach involving (among others) the calculation of terrain corrections to a suitable distance (e.g. 40km) from the measurement points.

A grid-based model parameterization was adopted. The seismic velocity and density grids were different allowing larger model cells for the receiver function method for deeper layers

and by allowing additional lateral padding in the density model for taking into account border effects.

Figure 3 shows the result of a simple series of experiments on synthetic data from a single interface. The full Zoeppritz equations were used to generate exact P_N and RF. In a noise-free case, both P inversion and joint P_N and RF inversion produce identical estimates of the fluctuations. However, when random noise was added to the P_N and RF values, the joint method becomes clearly superior. The simplest reason for this is that both methods constrain the same number of unknowns but the joint method uses twice as much data. This is much greater statistical leverage. As this figure shows, the f_J estimates are most dramatically improved in the joint inversion and that leads to better estimates of the pseudo-Poisson's ratio fluctuation $\tilde{f}_J f_J$.

FPJI - Joint Inversion Workflow

The velocity model building was performed since the first iteration by applying the simultaneous joint inversion of seismic refraction and receiver function data. This provided a long wavelength solution of the velocity field ranging from detailed velocity determinations to macro-velocity determinations for the model section below the maximum penetration of the long offset turning rays. The receiver function method was critical at this stage in extrapolating the velocity determinations to depth.

Further refinement of the velocity model for depth migration was performed by interpreting geologically consistent horizons, determining post-migration residuals along them and performing joint inversions in conjunction with receiver function. The horizon-based joint inversion proceeded in a layer stripping approach from top to bottom of the model (figure 4).

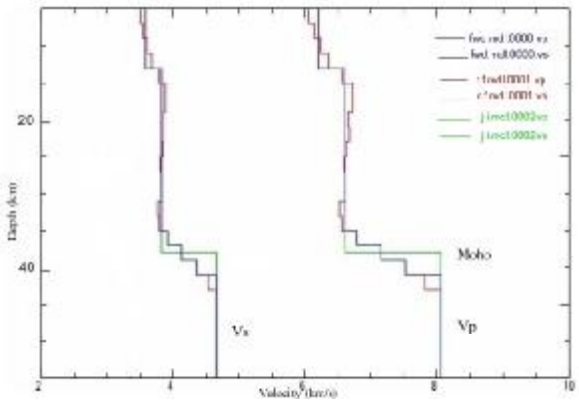

Figure 4. Velocity model building through Joint Inversion of seismic refraction and receiver function data, Central Iran.

Conclusions

The Joint-Inversion velocity model building workflow shows various advantages over traditional approaches. Some of these are:

1) The simultaneous use of receiver function data with seismic refraction provides extended depth resolution to what can be achieved from the use of the first breaks alone: from the first iterations one can solve for the macro velocities describing the whole model.
2) Receiver function data are equally sensitive to low and high density distributions whilst turning rays are more sensitive to high-velocity zones. This means that seismic refraction-receiver function joint inversion is able to retrieve near surface velocity inversions that would not be obtained by first break tomography alone.
3) The inversion problem becomes less non-unique and converges more rapidly toward the correct solution (velocity model building takes many less iterations and it is more reliable).

Acknowledgements
The author acknowledged IIEES (International Institute Earthquake Engineering and Seismology) of Iran, for providing the necessary data for this research. We thank Indago Petroleum Ltd and Ministry of Oil and Gas, Oman for allowing the publication of the real data application.

References

- Galve, A., Sapin, M., Hirn, A., Diaz, J., lepin, C., Laigle, M., Gallart.J., 2002. Complex images of Moho and variation of Vp/Vs across the Himalaya and Sounth Tibet, from a joint receiver function and ide angel reflection approach: J. Geophys. Res., no. 29, p. 2182-2186.
- Colombo, D., Mantovani, M., De Stefano, M., Garrad, D., and Al Lawati, H., 2007. Simultaneous joint inversion of seismic refraction and receiver function depth Migration in Northern Oman: Departement of Earth and Atmospherics Sciences, Saint Louis University, Sponsored by DSWA, Contract No. DSWA 01-100-c0160.
- Julià, J., Ammon, C.J., and Herrmann, R.B., 2003. Lithospheric structure of the Arabian Shield from the joint inversion of receiver functions and surface wave group velocities: Tectonophysics, no. 371, p. 1–21.
- Hu, J., Zhu, X., Xia, J., Chen, Y., 2005. Using surface wave and receiver function to jointly inverse the crust–mantle velocity structure in the West Yunnan area: Chin. J. Geophys, no. 48, p. 1069–1076.
- Chang, S., and Baag, C., 2005. Crustal structure in Southern Korea from joint analysis of teleseismic receiver functions and surface-wave dispersion: BSSA no. 95, p. 1516–1534.